Mass-Transfer Rate Enhancement for CO_2 Separation by Ionic Liquids: Theoretical Study on the Mechanism

Wenlong Xie
Dept. of Chemistry and Chemical Engineering, State Key Laboratory of Materials-Oriented Chemical Engineering, Nanjing Tech University, Nanjing 210009, P.R. China

Div. of Energy Science/Energy Engineering, Luleå University of Technology, 97187 Luleå, Sweden

Xiaoyan Ji
Div. of Energy Science/Energy Engineering, Luleå University of Technology, 97187 Luleå, Sweden

Xin Feng and Xiaohua Lu
Dept. of Chemistry and Chemical Engineering, State Key Laboratory of Materials-Oriented Chemical Engineering, Nanjing Tech University, Nanjing 210009, P.R. China

DOI 10.1002/aic.14932
Published online August 19, 2015 in Wiley Online Library (wileyonlinelibrary.com)

To promote the development of ionic liquid (IL) immobilized sorbents and supported IL membranes (SILMs) for CO_2 separation, the kinetics of CO_2 absorption/desorption in IL immobilized sorbents was studied using a novel method based on nonequilibrium thermodynamics. It shows that the apparent chemical-potential-based mass-transfer coefficients of CO_2 were in three regions with three-order difference in magnitude for the IL-film thicknesses in microscale, 100 nm-scale, and 10 nm-scale. Using a diffusion-reaction theory, it is found that by tailoring the IL-film thickness from microscale to nanoscale, the process was altered from diffusion-control to reaction-control, revealing the inherent mechanism for the dramatic rate enhancement. The extension to SILMs shows that the significant improvement of CO_2 flux can be obtained theoretically for the membranes with nanoscale IL-films, which makes it feasible to implement CO_2 separation by ILs with low investment cost. © 2015 American Institute of Chemical Engineers *AIChE J*, 61: 4437–4444, 2015
Keywords: CO_2 separation, ionic liquids, kinetics, immobilization, supported ionic liquid membranes

Introduction

Postcombustion CO_2 capture is an urgent and world-wide hot topic in both academic and industrial fields. A cost-effective CO_2 separation technology is crucial to make carbon capture and storage feasible to mitigate CO_2 emissions mainly from fossil-fuelled power plants. Ionic liquids (ILs)[1,2] have been proposed as promising solvents to conduct postcombustion CO_2 capture.[3] However, two crucial problems are still pending to industrialize IL-based technology in CO_2 separation, one is the low gas-liquid mass-transfer rate of CO_2 in ILs, the other is the high cost of ILs.[4]

IL immobilization into porous solid supports[5–9] and supported IL membranes (SILMs)[10–14] can significantly enhance the mass-transfer rate of CO_2 in ILs and reduce the amount of ILs needed for CO_2 separation.[15] However, for the IL immobilization, the available research work was focused on the experimental studies with a major purpose to obtain a high CO_2 absorption capacity along with the investigation of the effects of IL loadings and operational conditions (e.g., temperature).[5–9,16,17] Theoretical studies were on the correlation using classical kinetic and thermodynamic models[9,16] without any mechanism study, and how the IL-film thickness affects the mass-transfer rate cannot be revealed using such empirical methods. In addition, for SILMs, the reported low CO_2 permeability for the microscale membrane cannot meet the requirements of industrial applications.[18,19] Meanwhile, SILMs generally can only be operated at low trans-membrane pressures to avoid blowing ILs out of the pores in the support,[20] thus, a lot of research work has been conducted to enhance the membrane stability to achieve higher CO_2 permeability by operating the membrane process at relatively high pressures. Although the decrease of membrane thickness can lead to a high CO_2 mass-transfer rate or flux, the CO_2 permeability for a membrane with IL-film thickness down to nanoscale has not yet been studied. Therefore, further work needs to be carried out both experimentally and theoretically.

The objective of our work was to study the effect of IL-film thickness on the performance of CO_2 absorption/desorption in IL immobilized sorbents experimentally and theoretically. In the first part of this work,[21] the effect of IL-film thickness on CO_2 absorption/desorption processes with two IL impregnated titanium dioxide (P25) supported sorbents was studied experimentally. Using these experimental results and those from the literarure,[8] in this part, the kinetics of CO_2 absorption/desorption in IL immobilized sorbents was studied based on nonequilibrium thermodynamics, and the effect of IL-film thickness on the CO_2 mass-transfer rate was explored quantitatively. The mechanism behind was revealed using the diffusion-reaction theory. Based

Correspondence concerning this article should be addressed to X. Lu at xhlu@njtech.edu.cn.

on the analogue of CO_2 absorption/desorption in IL immobilized sorbents, the SILM process was further analyzed to seek for promising solutions solving the two pending crucial problems in CO_2 separation with IL-based technologies.

Theory

CO_2 absorption/desorption rate

The CO_2 absorption/desorption rate was described using Eq. 1

$$J_{CO_2} = \frac{dm_{CO_2,t}}{dt} \tag{1}$$

where J_{CO_2} is the absorption/desorption rate of CO_2 in P25-IL in mol CO_2/(mol IL min), $\mu CO_{2,t}$ is the amount of absorbed/desorbed CO_2 in P25-IL in mol CO_2/mol IL, and t is the time in min.

Chemical-potential-based mass-transfer coefficient k_μ

Nonequilibrium thermodynamics can be used to study the entropy generated by an irreversible process.[22,23] When the system is close to equilibrium, the linear relationship can be obtained between the flux and the driving force, which is termed as linear nonequilibrium thermodynamics.[24,25] The process of CO_2 absorption/desorption in IL-film studied in this work can be considered as a process which is close to equilibrium.[26] Based on linear nonequilibrium thermodynamics and using the chemical potential gradient ($\Delta\mu_{CO_2}$) instead of the concentration gradient as the driving force, we have[25,26]

$$J_{CO_2} = k_\mu \cdot \frac{\Delta\mu_{CO_2}}{RT} \tag{2a}$$

$$\frac{\Delta\mu_{CO_2}}{RT} = \frac{\mu_{CO_2,e}}{RT} - \frac{\mu_{CO_2,t}}{RT} \tag{2b}$$

Combing Eqs. 2a and b, we have

$$J_{CO_2} = k_\mu \cdot \left(\frac{\mu_{CO_2,e}}{RT} - \frac{\mu_{CO_2,t}}{RT}\right) \tag{2}$$

where k_μ is the apparent chemical-potential-based mass-transfer coefficient of a CO_2 absorption/desorption process, $\mu_{CO_2,e}$ and $\mu CO_{2,t}$ are the chemical potentials of CO_2 in IL at equilibrium and at time t, respectively, $\Delta\mu_{CO_2}$ is the chemical potential gradient, R is the gas constant, and T is the temperature in Kelvin. It is worth noting that the parameter k_μ has a certain physical meaning, not just a regression parameter.

The chemical potential of CO_2 in IL can be calculated according to Eq. 3a.

$$\mu_{CO_2}(T,p) = \mu^{\ominus}_{CO_2}(T,p) + RT\ln a_{CO_2} \tag{3a}$$

where $\mu^{\ominus}_{CO_2}(T,p)$ is the standard chemical potential, p is the partial pressure of CO_2, and a_{CO_2} is the activity of CO_2 in IL.

In this work, it was assumed that the nonideal behavior of CO_2 in IL can be neglected due to the low CO_2 solubility.[27] Following this assumption, the activity coefficient of CO_2 in an IL equals to one, and the activity of CO_2 in the IL equals to the corresponding concentration, that is, $\gamma_{CO_2} = 1$, $a_{CO_2} = x_{CO_2}$. Therefore, Eq. 3a can be simplified as

$$\mu_{CO_2}(T,p) = \mu^{\ominus}_{CO_2}(T,p) + RT\ln x_{CO_2} \tag{3b}$$

Based on Eqs. 2a, 2b and 3b, we have

$$\frac{\Delta\mu_{CO_2}}{RT} = \frac{\mu_{CO_2,e}}{RT} - \frac{\mu_{CO_2,t}}{RT} = \frac{1}{RT}\cdot\left(RT\ln x_{CO_2,e} - RT\ln x_{CO_2,t}\right) = \ln\left(x_{CO_2,e}/x_{CO_2,t}\right) \tag{4a}$$

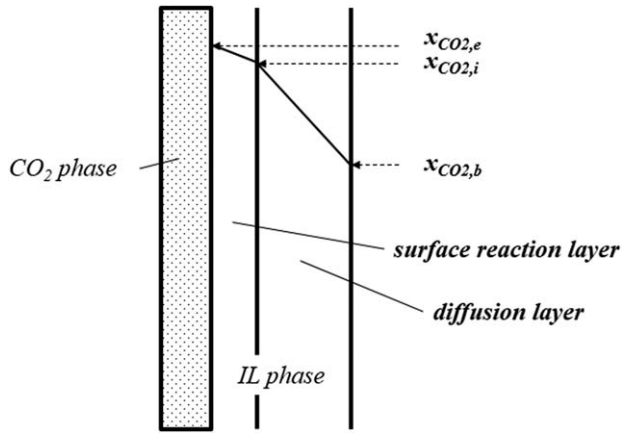

Figure 1. Schematic diagram of CO_2 absorption/desorption process in ILs.

$$J_{CO_2} = k_\mu \cdot \ln\left(x_{CO_2,e}/x_{CO_2,t}\right) \tag{4b}$$

Based on Eqs. 1 and 4b, we have

$$k_\mu = \frac{dm_{CO_2,t}/dt}{\ln\left(x_{CO_2,e}/x_{CO_2,t}\right)} \tag{4}$$

Diffusion-reaction theory

According to our previous work,[25,26,28–30] the CO_2 absorption/desorption process in IL was assumed to comprise two steps: surface-reaction and diffusion as described in Figure 1. In the surface-reaction layer, IL in sorbents contacts CO_2 in the vapor phase, CO_2 chemically or physically dissolves into IL. In the diffusion layer, the dissolved CO_2 is transported away from the interface through the surround liquids. The chemical potential of CO_2 in the gas phase equals to that in the liquid phase at equilibrium. Assuming that the average amount of absorbed CO_2 in IL ($x_{CO_2,b}$) was a boundary condition for the diffusion layer as shown in Figure 1 and considering that the nonideal behavior of CO_2 in IL was negligible,[27] the concentration of CO_2 in IL can be described as those shown in Figure 1, where $x_{CO_2,e}$, $x_{CO_2,i}$, and $x_{CO_2,b}$ represent the concentrations of CO_2 at equilibrium, in the interface and on the boundary of the diffusion layer. The overall resistance ($1/k_\mu$) of the process can be considered as the summation of the resistances from the reaction layer and diffusion layer as described in Eq. 5, in which $k_{\mu,s}$ is the surface-reaction chemical-potential-based mass-transfer coefficient and $k_{\mu,d}$ is the diffusion chemical-potential-based mass-transfer coefficient. The diffusion chemical-potential-based mass-transfer coefficient $k_{\mu,d}$ is related to the thickness of diffusion layer (h), that is, the IL-film thickness.

$$\frac{1}{k_\mu} = \frac{1}{k_{\mu,s}} + \frac{1}{k_{\mu,d}} \tag{5}$$

Results and Discussion

Apparent chemical-potential-based mass-transfer coefficient k_μ

The experimental results of CO_2 absorption/desorption in P25-ILs in the first part of this work[21] and those from Ref. 8 were used to study the kinetics of CO_2 mass transfer in immobilized IL sorbents. In Ref. 8, the CO_2 absorption in PMMA-[EMIM][Arg] was measured at 40°C, and the IL loadings were 20 wt %, 40 wt %, 60 wt %, and 100 wt %, respectively. The experimental conditions are summarized in Table 1.

Table 1. Summary of the Experimental Conditions for CO_2 Absorption/Desorption

Sorbent	IL Loadings (wt %)	Absorption/Desorption Temperature (°C)	Sources
P25-[APMIm]Br	25.8, 37.2, 40.4, 44.2, 55.9, 100	35/80	Ref. 21
P25-[BMIm]Ac	10.0, 19.0, 28.5, 38.2, 58.1	50/50	Ref. 21
PMMA-[EMIM][Arg]	20, 40, 60, 100	40/	Ref. 8

The experimental results of the absorbed/desorbed CO_2 in the immobilized IL sorbents were fitted to the following equation[31]

$$m_{CO_2,t}=At^B+C(1-e^{-Dt}) \tag{6}$$

where A, B, C, and D are constants in fitting.

Based on the amount of CO_2 absorbed/desorbed in the immobilized IL sorbents calculated with Eq. 6, the average amount of CO_2 absorbed/desorbed in the loaded IL was calculated and defined as the mole fraction of CO_2 at time t ($x_{CO_2,t}$, $x_{CO_2,t}=x_{CO_2,b}$) in the IL. The equilibrium solubility of CO_2 in the corresponding ILs at the corresponding temperatures ($x_{CO_2,e}$) was calculated based on data from Refs. 8, 32, and 33. The calculation results of $x_{CO_2,e}$ are summarized in Table 2.

Substituting Eq. 6 to Eq. 1, the CO_2 absorption/desorption rate can be calculated as

$$J_{CO_2}=dm_{CO_2,t}/dt=A\cdot Bt^{B-1}+C\cdot De^{-Dt} \tag{7}$$

Using Eq. 7, J_{CO_2} (or $dm_{CO_2,t}/dt$) was calculated. The ratio of $dm_{CO_2,t}/dt$ to $\ln(x_{CO_2,e}/x_{CO_2,t})$ was further calculated and illustrated in Figure 2. Except some cases in Figure 2e, all the curves are almost presented as linear lines, which imply that the slope of each curve is a constant. The nonlinear curves in Figure 2e can be attributed to the low temperature for the CO_2 desorption from P25-[BMIm]Ac. More discussion was given later.

Based on the analysis of linear nonequilibrium thermodynamics and the expression in Eq. 4, we can see that the slope is the apparent chemical-potential-based mass-transfer coefficient (k_μ). The obtained k_μ at each IL loading for different immobilized IL sorbents are listed in Tables 3–5.

For the CO_2 absorption in P25-[APMIm]Br with different IL loadings (i.e., different thickness of IL-films), the apparent chemical-potential-based mass-transfer coefficients (k_μ) present in three regions as shown in Figure 2a and listed in Table 3. For the thick IL-films (Region 3), the values of k_μ are very small, around 10^{-4}. For the medium thickness of IL-films (Region 2), the values of k_μ increase 100 times. When the thickness of IL-film further decreases (Region 1), the value of k_μ increases 10 times more compared to the medium thickness, and it is 1000 times higher compared to the thick IL-films. For the CO_2 absorption in P25-[BMIm]Ac and PMMA-[EMIM][Arg] with different IL loadings (i.e., different thicknesses of IL-films), the apparent chemical-potential-based mass-transfer coefficients (k_μ) also present in three regions, as shown in Figures 2b–2c and listed in Tables 4 and 5.

Table 2. Equilibrium Solubility of CO_2 in IL

IL	Temperature (°C)	[a]Capacity (mol CO_2/mol IL)	$x_{CO_2,e}$ mol CO_2/(mol CO_2 + mol IL)
[APMIm]Br	35/[b]80	0.50	0.33
[BMIm]Ac	50	0.256	0.204
[EMIM][Arg]	40	1.5	0.6

[a]Data from Refs. 8, 32, and 33.
[b]As almost all the absorbed CO_2 in [APMIm]Br at 35°C can be desorbed under desorption condition (80°C), the equilibrium solubility in desorption used in calculation is the same as in absorption.

For the CO_2 desorption in P25-[APMIm]Br with different IL loadings (i.e., different thicknesses of IL-films), the apparent chemical-potential-based mass-transfer coefficients (k_μ) also distribute in three regions as shown in Figure 2d and listed in Table 3. For the thick IL-films (Region 3), the values of k_μ are very small, around 10^{-4} to 10^{-3}. For the medium thickness of IL-films (Region 2), the values of k_μ increase about 100 times. When the thickness of IL-film further decreases (Region 1), the values of k_μ increase but not as much as those in the absorption processes.

For the CO_2 desorption in P25-[BMIm]Ac, when the [BMIm]Ac loading is less than 58.1 wt %, the apparent chemical-potential-based mass-transfer coefficients (k_μ) are not so much different as listed in Table 4, leading to two distinct regions as shown in Figure 2e. The reason might be that the chosen temperature for the CO_2 desorption in P25-[BMIm]Ac was not high enough to desorb all the absorbed CO_2, thus, affecting the kinetics. Therefore, the obtained k_μ for the CO_2 desorption in P25-[BMIm]Ac might not be as reliable as those in other cases.

The effect of IL-film thickness on k_μ

For the IL immobilized sorbents, the IL-film thickness is an essential parameter because it influences both the amount of CO_2 that can be absorbed in IL for a given surface area (i.e., the CO_2 equilibrium capacity) and the CO_2 mass-transfer rate.[5–9,16,17] To quantitatively study the effect of IL-film thickness on k_μ, the IL-film thicknesses of P25-[APMIm]Br estimated in the first part of this work[21] are also listed in Table 3, which clearly shows that the order of the apparent chemical-potential-based mass-transfer coefficient (k_μ) corresponds to the scale of the IL-film thickness.

The estimated film thicknesses of P25-[BMIm]Ac in the first part of this work[21] are listed in Table 4. For the CO_2 absorption in P25-[BMIm]Ac, similar observation can be obtained, that is, the order of k_μ is consistent with the scale of the IL-film thickness for most of cases. For the CO_2 desorption in P25-[BMIm]Ac, it has been mentioned in the former text that the temperature was not high enough to desorb all the absorbed CO_2, which causes the values of k_μ are not obviously different for most of the cases. Anyhow, the small value of k_μ for the case of 58.1 wt % IL corresponds to the thick IL-film (2 μm).

Combining the CO_2 absorption/desorption performance with the corresponding IL-film thickness, the mechanism behind can be revealed. Taking the CO_2 absorption/desorption in P25-[APMIm]Br as an example, if the IL-film is thicker than microscale (Region 3), that is, the IL-film thickness is in a level of millimeter or centimeter, the mass-transfer rate of CO_2 is very low. This can be the case that ILs are directly used as absorbents (where the IL-film thicknesses are mostly

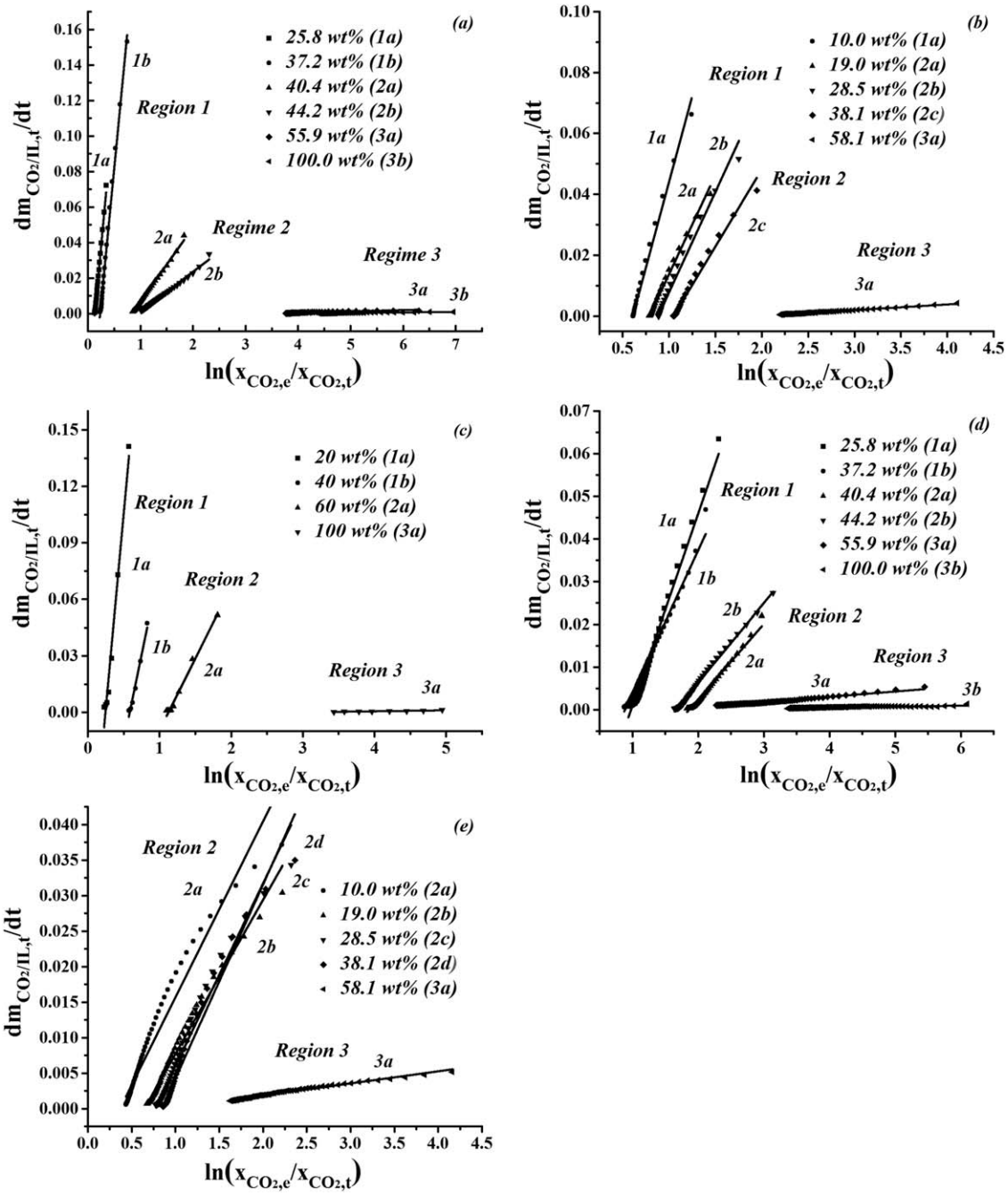

Figure 2. The $dm_{CO_2,t}/dt$ vs. $\ln(x_{CO_2,e}/x_{CO_2,t})$ for CO_2 absorption/desorption in immobilized IL sorbents.

(a), (d): P25-[APMIm]Br; (b), (e): P25-[BMIm]Ac; (c): PMMA-[EMIM][Arg].

in millimeter or centimeter) or the state-of-the-art SILMs (micrometer[12]), and it explains why the direct use of ILs in CO_2 absorption often suffers from a low rate and is infeasible for large-scale applications.[34] The cases distributed in Regions 2 and 1 in Figure 2 represent ILs being used as sorbents by immobilization on porous supports with microscale or

Table 3. Apparent Chemical-Potential-Based Mass-Transfer Coefficient k_μ for CO_2 in P25-[APMIm]Br and the Corresponding IL-Film Thickness[21]

Loading (wt %)	k_μ at 35°C Absorption	k_μ at 80°C Desorption	Film Thickness[21] (nm)	Scale of Film Thickness
25.8	0.318	4.49×10^{-2}	17.5	~10 nm
37.2	0.306	3.35×10^{-2}	25.5	
40.4	4.18×10^{-2}	1.77×10^{-2}	54.5	~100 nm
44.2	2.24×10^{-2}	1.86×10^{-2}	63.6	
55.9	7.86×10^{-4}	1.24×10^{-3}	1.64×10^{3}	~2 μm
100	3.24×10^{-4}	2.19×10^{-4}	2.50×10^{6}	~2 mm

Table 4. Apparent Chemical-Potential-Based Mass-Transfer Coefficient k_μ for CO_2 in P25-[BMIm]Ac at 50°C and the Corresponding IL-Film Thickness[21]

Loading (wt %)	k_μ Absorption	k_μ Desorption	Film Thickness[21] (nm)	Scale of Film Thickness
10.0	0.113	2.48×10^{-2}	2.9	~10 nm
19.0	6.51×10^{-2}	2.17×10^{-2}	8.9	
28.5	6.60×10^{-2}	2.57×10^{-2}	36.7	~100 nm
38.2	5.06×10^{-2}	2.73×10^{-2}	97.5	
58.1	1.87×10^{-3}	1.71×10^{-3}	2.81×10^{3}	~2 μm

nanoscale IL-films, and the CO_2 absorption/desorption was significantly enhanced being acceptable for practical applications.

Based on the above analysis, we can conclude that the nanoscale IL-film is necessary to achieve an acceptable absorption/desorption rate for practical applications. This is crucial information for the SILM process. However, the IL-film thickness for the state-of-the-art SILMs is still in microscale,[12] and further improvement can be achieved by decreasing the IL-film thickness to nm-level based on the above analysis.

$k_{\mu,s}$ and $k_{\mu,d}$

The results in the foregoing section showed that the CO_2 mass-transfer rate can be dramatically enhanced when the IL-film thickness was tailored down to nanoscale. To understand it, the CO_2 absorption in P25-[APMIm]Br at 35°C was chosen as an example for further analysis in this section. Figure 3 shows the chemical-potential-based mass-transfer coefficient k_μ of CO_2 in P25-[APMIm]Br with different IL-film thickness at 35°C. The value of k_μ increases with decreasing IL-film thickness. When the IL-film thickness is in microscale (Region 3), the increasing rate of k_μ is the same as the decreasing rate of IL-film thickness. For example, when the IL-film thickness decreases from 1640 nm to 63.6 nm (26 times), k_μ increases 28 times. In Regions 2 and 1, the film thickness is in nanoscale, the increasing rate of k_μ is much faster than the decreasing rate of IL-film thickness, and a slight decrease of IL-film thickness leads to a remarkable increase of k_μ. For example, when the film thickness deceases from 63.6 nm to 25.5 nm (2 times), k_μ increases 14 times.

The CO_2 chemical-potential-based mass-transfer coefficient k_μ represents the overall resistance ($1/k_\mu$) for CO_2 absorption in IL immobilized sorbents. Based on the diffusion-reaction model, this overall resistance is the summation of the resistances from the reaction and diffusion layers. Generally, the resistance from the reaction layer depends on the temperature, while the resistance from the diffusion layer depends on the IL-film thickness. The effect of the IL-film thickness (h) on

Table 5. Apparent Chemical-Potential-Based Mass-Transfer Coefficient k_μ for CO_2 in PMMA-[EMIM][Arg] at 40°C

Loading (wt %)	k_μ, Absorption
20	0.414
40	0.185
60	7.63×10^{-2}
100	5.47×10^{-4}

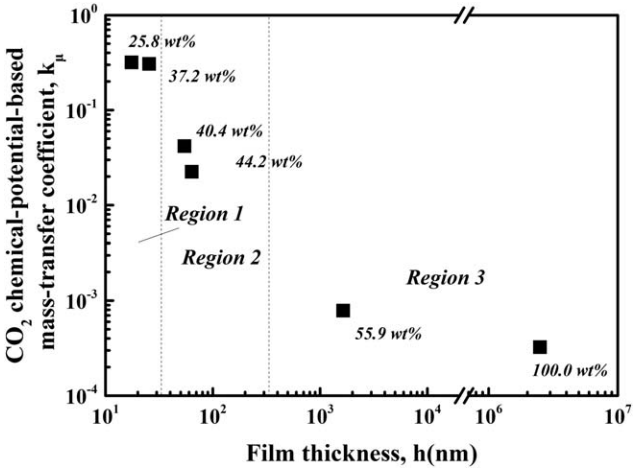

Figure 3. CO_2 chemical-potential-based mass-transfer coefficient k_μ in P25-[APMIm]Br with different IL-film thickness at 35°C.

the overall resistance ($1/k_\mu$) for the CO_2 absorption in P25-[APMIm]Br at 35°C is illustrated in Figure 4, which shows that the overall resistance ($1/k_\mu$) decreases with decreasing IL-film thickness and approaches a constant when the film thickness decreases down to nanoscale. This observation implies that $k_{\mu,s}$ is the main factor to control the CO_2 mass transfer when the IL-film thickness is very thin. Assuming that the contribution of $1/k_{\mu,d}$ to $1/k_\mu$ can be neglected compared to $1/k_{\mu,s}$ for the very thin film, $k_{\mu,s}$ was obtained based on the results illustrated in Figure 4 with the value of 0.358, that is, $k_{\mu,s} = 1/2.79 = 0.358$.

It is worth mentioning that for the loading of 55.9 wt % and pure [APMIm]Br (Region 3), the mass-transfer rate was very low, and the contribution of the resistance from the reaction layer to the overall resistance was very small. To obtain more reliable results for the resistance of reaction layer, the experimental results with the loading of 55.9 wt % and pure [APMIm]Br were excluded in data processing in Figure 4.

Assuming the temperature-dependent $k_{\mu,s}$ is independent of IL-film thickness, the resistance from the diffusion layer with different thickness can be obtained based on Eq. 5 with the value of k_μ (absorption) listed in Table 3 and $k_{\mu,s} = 0.358$. The

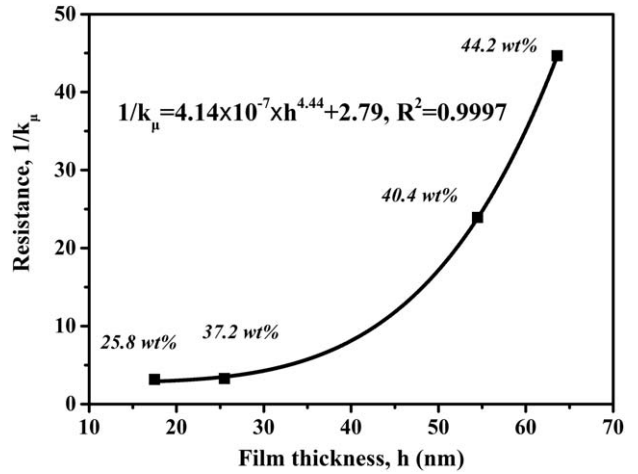

Figure 4. Resistance of CO_2 mass transfer in P25-[APMIm]Br with different IL-film thickness at 35°C.

Table 6. Resistances for the CO_2 Mass Transfer in P25-[APMIm]Br at 35°C

Film Thickness (nm)	Overall Resistance	Diffusion Resistance (%)	Reaction Resistance (%)
17.5	3.14	11.4	88.6
25.5	3.27	14.7	85.3
54.5	23.92	88.4	11.6
63.6	44.64	93.8	6.2
1640	1272.27	99.8	0.2
2,500,000	3086.42	99.9	0.1

contributions of the resistances from the reaction and diffusion layers to the overall resistance of the CO_2 absorption in P25-[APMIm]Br at 35°C were further calculated as listed in Table 6. As it can be seen, the process was switched from the diffusion control to surface-reaction control, and the decrease of IL-film thickness down to nanoscale resulted in a dramatic decrease of the overall resistance due to the dramatic decrease of the resistance from the diffusion layer. For example, when the IL-film thickness is 2.5 μm, the overall resistance is 3086, and the resistance from the diffusion layer ($1/k_{\mu,d}$) contributes 99.9% to the overall; while the diffusion layer contributes only 11.4 % (10 times lower) when the IL-film thickness decreases down to 17.5 nm, and the overall resistance decreases down to 3.14. This further explains the rate enhancement for the process with a nanoscale IL-film.

Extension to SILMs

SILMs have showed great potential in CO_2 separation because of the high contact surface area, the low amount of IL required, and the enhanced mass-transfer rate.[10–14] As mentioned previously that the IL-film thicknesses in SILMs are mostly in micrometer.[12] Based on the results obtained in this work, the performance of SILMs can be further improved by decreasing the thickness of IL-film. The results also showed that the high mass-transfer rate of CO_2 can be achieved with the IL-film in nanoscale, but what is the CO_2 flux and the corresponding equipment size if the IL-film goes down to nanoscale for SILMs?

To address the above questions, an estimation of the CO_2 flux in the SILM with [BMIm]Ac was conducted because of the available experimental CO_2 solubility in [BMIm]Ac. The estimation of the CO_2 mass-transfer rate in the SILMs was based on the following assumptions:

1. The transport through the SILMs followed the dissolution/diffusion mechanism;[19,35]

2. The effect of the pressure on the apparent chemical-potential-based mass-transfer coefficient k_μ was negligible.

Therefore, for the SILM with [BMIm]Ac, the apparent chemical-potential-based mass-transfer coefficient was set to be that of CO_2 absorption in P25-[BMIm]Ac as listed in Table 4. The partial pressures of CO_2 on the feed and permeate sides were set to be 1 (p_f) and 0.5 bar (p_p), respectively. The operational temperature was set to be 50°C. Assuming that the chemical potential gradient was the driving force across the membrane,[36,37] the flux can be calculated based on Eqs. 8 and 3b

Table 7. CO_2 Mass-Transfer Rate in Supported [BMIm]Ac IL Membranes

Membrane Thickness (nm)	~3000	~100	~10	[a]12,250
CO_2 mass-transfer rate (kg/(m^2 h))	3.87	105	135	0.01

[a]This data was obtained from Ref. 38 with [emim][Ac] supported on Al_2O_3/TiO_2.

Table 8. Membrane Area and Amount of IL Needed for SILM with [BMIm]Ac at 50°C with a 0.5 ton/h CO_2 Recovery Capacity

Thickness of IL (nm)	~3000	~100	~10
Mass-transfer rate of CO_2 (kg/m^2/h)	3.87	105	135
Volume of IL needed (L)	0.364	4.65×10^{-4}	3.29×10^{-5}
[a]Membrane needed (m^2)	323	11.9	9.28
[b]Amount of HF membrane tubes needed	68,500	2530	1970

[a]The effective area of IL on membrane was assumed as 40% in this calculation.
[b]Size of single HF membrane tube: inner diameter = 2 mm, outer diameter = 3 mm, height = 0.5 m.

$$J_{CO_2} = k_\mu \cdot \left(\frac{\mu_{CO_2,f}}{RT} - \frac{\mu_{CO_2,p}}{RT}\right) \tag{8}$$

where $\mu_{CO_2,f}$ and $\mu_{CO_2,p}$ are the chemical potentials of CO_2 in IL on the feed and permeate sides, respectively.

The results listed in Table 7 show that the CO_2 mass-transfer rate is enhanced by 100 times when the thickness of IL membrane is decreased from microscale to nanoscale, that is, the process is changed from diffusion-control to reaction-control. The quantitative estimation and analysis in this work reveal that the decrease of IL membrane thickness is of great potential in enhancing the mass-transfer rate of CO_2 in IL membranes.

The equipment size and the amount of IL needed in SILM were further estimated and compared with the amine scrubbing process constructed at Huaneng Beijing power plant.[39,40] For the chosen amine scrubbing process, 20 % MEA solution was used as the absorbent and the CO_2 recovery capacity was 0.5 ton/h. The process consisted of a chemical-absorption-based absorber (inner diameter = 1.2 m, height = 31 m) and a stripper (inner diameter = 1 m, height = 30 m) for the solvent regeneration. Both the absorber and the stripper had two 7.5 m-high packing levels.

Using SILMs with the same CO_2 recovery capacity, the membrane area and the amount of ILs were estimated as listed in Table 8. The estimation shows that only thousands of hollow fiber (HF) membrane tubes and a small amount of IL (about 0.03 mL) are needed when the thickness of IL membrane is in nanoscale. Compared to the large equipment and plenty amount of amine required in the scrubbing process, the SILMs with IL-film thickness in nanoscale obviously have great potential in reducing the CO_2 separation cost.

Furthermore, this quantitative investigation shows again that the decrease of the membrane thickness is of great potential in reducing the investment cost on equipment and materials. Therefore, by tailoring the IL-film thickness from microscale to nanoscale and then altering the process from diffusion-control to reaction-control, the low mass-transfer rate of CO_2 and the high price of IL can be potentially overcome. This gives a promising future in reducing the investment cost on equipment and materials (IL) and sheds light on solving the two pending crucial problems in CO_2 separation with IL-based technologies. Further work on the fabrication of nanoscale membrane and its application in CO_2 separation are on-going in our research group.

Conclusions

In this work, the CO_2 absorption/desorption in IL immobilized sorbents was studied theoretically. The results showed

that the apparent chemical-potential-based mass-transfer coefficient of the whole CO_2 absorption/desorption process in IL immobilized sorbents was in three distinct regions with 1000-time difference in magnitude depending on IL-film thickness on supports from microscale, 100 nm-scale to 10 nm-scale. The analysis based on the diffusion-reaction theory revealed the inherent mechanism for the rate enhancement, that is, these three distinct regions of the CO_2 mass-transfer rate correspond to diffusion-control and reaction-control processes with IL-film thicknesses in microscale, 100 nm-scale and 10 nm-scale, respectively. The extension to SILMs showed that a dramatic improvement of CO_2 flux can be achieved theoretically for membranes with nanoscale IL-films, and the equipment size and materials (IL) needed can be dramatically reduced. This gives a promising future in reducing the investment cost on equipment and materials (IL) and sheds light on solving the two pending crucial problems in CO_2 separation with IL-based technologies. Although the types of ILs investigated in this work are limited, the mechanism revealed has ubiquity to other ILs. The theoretical work can be extended to other gases, which will be the focus of our future work.

Acknowledgments

This work was financially supported by National 973 Key Basic Research Development Planning Program (2013CB733500), Major Research Projects of National Natural Science Fund (91334202), Major Research Program of National Natural Science Fund (21490584), Key Project of National Natural Science Foundation (21136004), National Natural Science Foundation (21176112) of China and the Project of Priority Academic Program Development of Jiangsu Higher Education Institutions (PAPD). The authors would like to thank Dr. Yuanhui Ji in TU Dortmund and Dr. Rong An in North Carolina State University for useful discussions regarding preparation of this manuscript.

Literature Cited

1. Blanchard LA, Hancu D, Beckman EJ, Brennecke JF. Green processing using ionic liquids and CO_2. *Nature*. 1999;399:28–29.
2. Bates ED, Mayton RD, Ntai I, Davis JH. CO_2 capture by a task-specific ionic liquid. *J Am Chem Soc*. 2002;124:926–927.
3. Rochelle GT. Amine scrubbing for CO_2 capture. *Science*. 2009;325:1652–1654.
4. Ramdin M, de Loos TW, Vlugt TJ. State-of-the-art of CO_2 capture with ionic liquids. *Ind Eng Chem Res*. 2012;51:8149–8177.
5. Zhang J, Zhang S, Dong K, Zhang Y, Shen Y, Lv X. Supported absorption of CO_2 by tetrabutylphosphonium amino acid ionic liquids. *Chemistry*. 2006;12:4021–4026.
6. Ren J, Wu L, Li B. Preparation and CO_2 sorption/desorption of N-(3-aminopropyl) aminoethyl tributylphosphonium amino acid salt ionic liquids supported into porous silica particles. *Ind Eng Chem Res*. 2012;51:7901–7909.
7. Vicent-Luna JM, Gutierrez-Sevillano JJ, Anta JA, Calero S. Effect of room-temperature ionic liquids on CO_2 separation by a Cu-BTC metal-organic framework. *J Phys Chem C*. 2013;117:20762–20768.
8. Wang X, Akhmedov NG, Duan Y, Luebke D, Li B. Immobilization of amino acid ionic liquids into nanoporous microspheres as robust sorbents for CO_2 capture. *J Mater Chem*. 2013;1:2978–2982.
9. Wang XF, Akhmedov NG, Duan YH, Luebke D, Hopkinson D, Li BY. Amino acid-functionalized ionic liquid solid sorbents for post-combustion carbon capture. *ACS Appl Mater Interfaces*. 2013;5:8670–8677.
10. Scovazzo P, Visser AE, Davis JH Jr, Rogers RD, Koval CA, DuBois DL, Noble RD. Supported ionic liquid membranes and facilitated ionic liquid membranes. *ChemInform*. 2002;33:240–240.
11. Noble RD, Gin DL. Perspective on ionic liquids and ionic liquid membranes. *J Membr Sci*. 2011;369:1–4.
12. Luis P, Van Gerven T, Van der Bruggen B. Recent developments in membrane-based technologies for CO_2 capture. *Prog Energy Combust Sci*. 2012;38:419–448.
13. Lozano L, Godinez C, De los Rios A, Hernandez-Fernandez F, Sanchez-Segado S, Alguacil F. Recent advances in supported ionic liquid membrane technology. *J Membr Sci*. 2011;376:1–14.
14. Bara JE, Carlisle TK, Gabriel CJ, Camper D, Finotello A, Gin DL, Noble RD. Guide to CO_2 separations in imidazolium-based room-temperature ionic liquids. *Ind Eng Chem Res*. 2009;48:2739–2751.
15. Samanta A, Zhao A, Shimizu GKH, Sarkar P, Gupta R. Post-combustion CO_2 capture using solid sorbents: a review. *Ind Eng Chem Res*. 2012;51:1438–1463.
16. Zhang Z, Wu L, Dong J, Li B, Zhu S. Preparation and SO_2 sorption/desorption behavior of an ionic liquid supported on porous silica particles. *Ind Eng Chem Res*. 2009;48:2142–2148.
17. Khan NA, Hasan Z, Jhung SH. Ionic liquids supported on metal-organic frameworks: remarkable adsorbents for adsorptive desulfurization. *Chemistry*. 2014;20:376–380.
18. Nguyen PT, Voss BA, Wiesenauer EF, Gin DL, Noble RD. Physically gelled room-temperature ionic liquid-based composite membranes for CO_2/N_2 separation: effect of composition and thickness on membrane properties and performance. *Ind Eng Chem Res*. 2012;52:8812–8821.
19. Scovazzo P. Determination of the upper limits, benchmarks, and critical properties for gas separations using stabilized room temperature ionic liquid membranes (SILMs) for the purpose of guiding future research. *J Membr Sci*. 2009;343:199–211.
20. Voss BA, Bara JE, Gin DL, Noble RD. Physically gelled ionic liquids: solid membrane materials with liquidlike CO_2 gas transport. *Chem Mater*. 2009;21:3027–3029.
21. Xie W, Ji X, Feng X, Lu X. Mass transfer rate enhancement for CO_2 separation using ionic liquids: experimental study on the influence of film thickness. *AIChE J*. Under review.
22. Prigogine I. Modération et transformations irreversibles des systemes ouverts. *Bulletin de la Classe des Sciences., Academie Royale de Belgique*. 1945;31:600–606.
23. Prigogine I. Etude thermodynamique des processus irréversibles. *Desoer*, *Liege*. 1947.
24. Demirel YA, Sandler SI. Nonequilibrium thermodynamics in engineering and science. *J Phys Chem B*. 2004;108:31–43.
25. Lu X, Ji Y, Liu H. Non-equilibrium thermodynamics analysis and its application in interfacial mass transfer. *Sci China Chem*. 2011;54:1659–1666.
26. Lu X, Ji Y, Feng X, Ji X. Methodology of non-equilibrium thermodynamics for kinetics research of CO_2 capture by ionic liquids. *Sci China Chem*. 2012;55:1079–1091.
27. Liu HJ, Tian H, Yao H, Yu DW, Zhao W, Bai XL. Improving physical absorption of carbon dioxide by ionic liquid dispersion. *Chem Eng Technol*. 2013;36:1402–1410.
28. Liu C, Ji Y, Shao Q, Feng X, Lu X. Thermodynamic analysis for synthesis of advanced materials. *Struct Bond*. 2009;131:193–270.
29. Ji Y, Ji X, Liu C, Feng X, Lu X. Modelling of mass transfer coupling with crystallization kinetics in microscale. *Chem Eng Sci*. 2010;65:2649–2655.
30. Ji X, Chen D, Wei T, Lu X, Wang Y, Shi J. Determination of dissolution kinetics of K_2SO_4 crystal with ion selective electrode. *Chem Eng Sci*. 2001;56:7017–7024.
31. Monazam ER, Shadle LJ, Miller DC, Pennline HW, Fauth DJ, Hoffman JS, Gray ML. Equilibrium and kinetics analysis of carbon dioxide capture using immobilized amine on a mesoporous silica. *AIChE J*. 2012;59:923–935.
32. Wu Y, Jiao Z, Wang G, Wu Y, Zhang Z. Synthesis, characterization and absorption efficiency of an ionic liquid for the absorption of CO_2. *Fine Chem*. 2007;24:324–327.
33. Shiflett MB, Kasprzak DJ, Junk CP, Yokozeki A. Phase behavior of {carbon dioxide+ [bmim][Ac]} mixtures. *J Chem Thermodyn*. 2008;40:25–31.
34. Hasib-ur-Rahman M, Siaj M, Larachi F. Ionic liquids for CO_2 capture-development and progress. *Chem Eng Process*. 2010;49:313–322.
35. Privalova EI, Mäki-Arvela P, Murzin DY, Mikkhola J-P. Capturing CO_2: conventional versus ionic-liquid based technologies. *Russ Chem Rev*. 2012;81:435–457.

36. Neves LA, Crespo JG, Coelhoso IM. Gas permeation studies in supported ionic liquid membranes. *J Membr Sci*. 2010;357:160–170.
37. Iarikov DD, Hacarlioglu P, Oyama ST. Supported room temperature ionic liquid membranes for CO_2/CH_4 separation. *Chem Eng J*. 2011; 166:401–406.
38. Albo J, Yoshioka T, Tsuru T. Porous Al_2O_3/TiO_2 tubes in combination with 1-ethyl-3-methylimidazolium acetate ionic liquid for CO_2/N_2 separation. *Sep Purif Technol*. 2014;122:440–448.
39. Huang B, Xu SS, Gao SW, Liu LB, Tao JY, Niu HW, Cai M, Cheng JA. Industrial test and techno-economic analysis of CO_2 capture in Huaneng Beijing coal-fired power station. *Appl Energy*. 2010;87:3347–3354.
40. Huang B, Xu S, Gao S, Liu L, Tao J, Niu H, Cai M, Cheng J. Industrial test of CO_2 capture in huaneng beijing coal-fired power station. *P CSEE*. 2009;17:004.

Manuscript received Jan. 25, 2015, and revision received June 16, 2015.